Personalized Medicine and Imaging

Clinical Cancer Research

^{89}Zr-Lumretuzumab PET Imaging before and during HER3 Antibody Lumretuzumab Treatment in Patients with Solid Tumors

Frederike Bensch[1], Laetitia E. Lamberts[1], Michaël M. Smeenk[1], Annelies Jorritsma-Smit[2], Marjolijn N. Lub-de Hooge[2,3], Anton G.T. Terwisscha van Scheltinga[2], Johan R. de Jong[3], Jourik A. Gietema[1], Carolien P. Schröder[1], Marlene Thomas[4], Wolfgang Jacob[4], Keelara Abiraj[5], Celine Adessi[5], Georgina Meneses-Lorente[6], Ian James[7], Martin Weisser[4], Adrienne H. Brouwers[3], and Elisabeth G.E. de Vries[1]

Abstract

Purpose: We evaluated biodistribution and tumor targeting of ^{89}Zr-lumretuzumab before and during treatment with lumretuzumab, a human epidermal growth factor receptor 3 (HER3)–targeting monoclonal antibody.

Experimental Design: Twenty patients with histologically confirmed HER3-expressing tumors received ^{89}Zr-lumretuzumab and underwent positron emission tomography (PET). In part A, ^{89}Zr-lumretuzumab was given with additional, escalating doses of unlabeled lumretuzumab, and scans were performed 2, 4, and 7 days after injection to determine optimal imaging conditions. In part B, patients were scanned following tracer injection before (baseline) and after a pharmacodynamic (PD)-active lumretuzumab dose for saturation analysis. HER3 expression was determined immunohistochemically in skin biopsies. Tracer uptake was calculated as standardized uptake value (SUV).

Results: Optimal PET conditions were found to be 4 and 7 days after administration of ^{89}Zr-lumretuzumab with 100-mg unlabeled lumretuzumab. At baseline using 100-mg unlabeled lumretuzumab, the tumor SUVmax was 3.4 (±1.9) at 4 days after injection. SUVmean values for normal blood, liver, lung, and brain tissues were 4.9, 6.4, 0.9 and 0.2, respectively. Saturation analysis ($n = 7$) showed that 4 days after lumretuzumab administration, tumor uptake decreased by 11.9% (±8.2), 10.0% (±16.5), and 24.6% (±20.9) at PD-active doses of 400, 800, and 1,600 mg, respectively, when compared with baseline. Membranous HER3 was completely downregulated in paired skin biopsies already at and above 400-mg lumretuzumab.

Conclusions: PET imaging showed biodistribution and tumor-specific ^{89}Zr-lumretuzumab uptake. Although, PD-active lumretuzumab doses decreased ^{89}Zr-lumretuzumab uptake, there was no clear evidence of tumor saturation by PET imaging as the tumor SUV did not plateau with increasing doses. *Clin Cancer Res; 23(20); 6128–37. ©2017 AACR.*

Introduction

The members of the human epidermal growth factor receptor (HER) family play a critical role in tumor growth, proliferation, and progression in multiple epithelial malignancies (1). Due to its lack of intrinsic tyrosine kinase activity and its need for dimerization partners, the role of HER3 in cancer, however, has long been unclear. HER3 is physiologically expressed in normal human tissues, such as the gastrointestinal, urinary, respiratory, and reproductive tract and skin (2). In multiple cancer types, HER3 overexpression has been linked with poor prognosis which increased interest in HER3 as potential target in cancer therapy (3–9).

Lumretuzumab (RG7116, RO5479599) is a glycoengineered humanized monoclonal antibody directed against the extracellular domain of HER3, displacing its ligand and inhibiting heterodimerization and downstream signaling. Furthermore, the antibody can cause direct cell death through antibody-dependent cellular cytotoxicity (10). A phase I study in patients with HER3-positive solid tumors of epithelial origin showed that lumretuzumab monotherapy was well tolerated and signs of clinical activity were reported (11).

Several challenges hamper early clinical development of novel molecular tumor-targeting agents. First, intra- and intertumor heterogeneity with regard to target expression is likely an important contributor to treatment failure (12–19). Second, finding the optimal dose and dosing schedule of antibodies in a dose

[1]Department of Medical Oncology, University of Groningen, University Medical Center Groningen, the Netherlands. [2]Department of Clinical Pharmacy and Pharmacology, University of Groningen, University Medical Center Groningen, the Netherlands. [3]Department of Nuclear Medicine and Molecular Imaging, University of Groningen, University Medical Center Groningen, the Netherlands. [4]Pharma Research and Early Development, Roche Innovation Center Munich, Penzberg, Germany. [5]Pharma Research and Early Development, Roche Innovation Center Basel, Basel, Switzerland. [6]Pharma Research and Early Development, Roche Innovation Center Welwyn, Welwyn, United Kingdom. [7]A4P Consulting Ltd, Sandwich, United Kingdom.

Note: Supplementary data for this article are available at Clinical Cancer Research Online (http://clincancerres.aacrjournals.org/).

F. Bensch and L.E. Lamberts contributed equally to this article.

Corresponding Author: Elisabeth G.E. de Vries, University of Groningen, University Medical Center Groningen, P.O. Box 30.001, 9700 RB Groningen, the Netherlands. Phone: 0031-503612934; Fax: 0031-503614862; E-mail: e.g.e.de.vries@umcg.nl

doi: 10.1158/1078-0432.CCR-17-0311

Translational Relevance

The human epidermal growth factor receptor 3 (HER3) plays an important role in tumor growth, proliferation, and progression. The humanized, HER3-targeting monoclonal, glycoengineered antibody lumretuzumab is in development for treatment of patients with HER3-positive solid tumors. Challenges in drug development include obtaining information concerning drug biodistribution, target occupancy, and intra- and interpatient tumor heterogeneity. In this study, assessment of biodistribution and visualization of tumor lesions was feasible with ^{89}Zr-lumretuzumab PET. Highest uptake in normal tissues was observed in the liver. Tumor tracer uptake varied between and within patients possibly reflecting intrapatient heterogeneity. Serial imaging at baseline and after the first pharmacodynamically active lumretuzumab dose showed decreased tumor uptake already after 400 mg, however, without plateauing. This study supports serial antibody PET-imaging during early clinical development to determine biodistribution and obtain insight into effects of different antibody doses on tumor targeting.

escalation study with a limited number of (heterogeneous) patients is challenging given potentially high intra- and interindividual variance in blood pharmacokinetics (PK). Due to limited or no side effects even at high doses, traditional approaches focusing on dose-limiting toxicities do not provide sufficient guidance (20). Finally, assumptions concerning the biodistribution of new drugs are often only based on blood PK, whereas information concerning the antibody level in the tumor lesions and target saturation at different doses is lacking.

By labeling antibodies with zirconium-89 (^{89}Zr), positron emission tomography (PET) can be performed. This technique can assess target expression noninvasively at a whole body level and determine the biodistribution of the administered antibody (21). Over 15 therapeutic antibodies have already been labeled with ^{89}Zr and tested in clinical trials (21–29). Performing serial PET scans before and during treatment allows investigation of target accessibility during treatment and may therefore be used to assess whether target saturation has been achieved. Based on antibody characteristics, radioactive decay, and dose of ^{89}Zr, a second tracer injection followed by a series PET scans can be performed 14 days after the first (24, 26).

First, we labeled the anti–HER3-antibody lumretuzumab with ^{89}Zr with high specific activity and radiochemical purity. Subsequently, in human tumor-bearing mice, we showed that ^{89}Zr-lumretuzumab specifically accumulated in HER3-expressing tumors related to HER3 expression levels (30).

This resulted in the clinical trial in which we determined the biodistribution and tumor targeting characteristics of ^{89}Zr-lumretuzumab before and during lumretuzumab treatment, including assessment of target saturation, and comparing these to serum PK and skin biopsies to evaluate pharmacodynamic (PD) effects.

Patients and Methods

Patient population

Patients with histologically confirmed locally advanced or metastatic HER3-expressing solid tumors of epithelial origin for whom no standard therapy existed were eligible for this study. Other eligibility criteria included age $\geq$ 18 years, written informed consent, Eastern Cooperative Oncology Group (ECOG) performance status of 0–2 and adequate hematologic (neutrophil count $\geq 1.5 \times 10^9$/L, platelet count $\geq 100 \times 10^9$/L, hemoglobin $\geq$ 10 g/dL), liver [bilirubin $\leq 1.5 \times$ upper limit of normal (ULN), aspartate aminotransferase/alanine aminotransferase $\leq 2.5 \times$ ULN, in case of liver metastases $\leq 5 \times$ ULN], and renal function (serum creatinine $\leq 1.5 \times$ ULN). Patients with significant concomitant diseases, active infections, current high doses of systemic corticosteroids, or symptomatic central nervous system primary tumors or metastases were excluded. Patients with previously unknown, asymptomatic brain metastases, which were detected on ^{89}Zr-lumretuzumab PET, were allowed to remain on the study according to the investigator's judgment unless radiotherapy for brain metastases was indicated.

This study was centrally approved by the Medical Ethical Committee of the Netherlands Cancer Institute and the Central Committee on Research Involving Human Subjects. All patients provided written informed consent. It was registered as part of the phase I study (ClinicalTrials.gov identifier NCT01482377).

HER3 expression in archival and freshly obtained tumor and skin samples

HER3 membrane expression was assessed centrally in biopsies from metastases to confirm patient eligibility for entry into the study and in skin biopsies at baseline and after the first PD-active dose using a validated immunohistochemistry (IHC) assay (Ventana Benchmark XT platform, primary antibody HER3 monoclonal antibody clone 7.3.8; Source Bioscience Ltd). HER3 positivity was defined as any positive membrane staining with a minimum of 100 neoplastic cells being evaluated. IHC was assessed semi-quantitatively using an immunoreactive score (IRS) according to: IRS = staining intensity (SI) x percent tumor cells stained (PS), where SI = 1 x "+" score + 2 x "++" score + 3 x "+++" score)/100 and PS = ("+" score + "++" score + "+++" score)/100.

Study design

This single-center, open-label, imaging study was performed at the University Medical Center Groningen (UMCG), the Netherlands.

Clinical grade ^{89}Zr-lumretuzumab was produced at the UMCG essentially as described previously (30, 31). In part A, the optimal imaging dose and schedule for ^{89}Zr-lumretuzumab PET imaging were assessed, and in part B, patients underwent two series of ^{89}Zr-lumretuzumab PET to analyze the biodistribution of ^{89}Zr-lumretuzumab and to determine the dose of unlabeled PD-active lumretuzumab required to achieve maximal or optimal tumor saturation.

In part A, a fixed dose of 37 MBq ^{89}Zr-lumretuzumab ($\sim$1 mg) was given with additional, escalating doses of unlabeled lumretuzumab in cohorts of two to three patients. The unlabeled lumretuzumab was administered over 15 minutes via an intravenous infusion, before ^{89}Zr-lumretuzumab bolus injection. After tracer injection, patients were observed for 4 hours for infusion-related reactions. PET scans in combination with low-dose CT scans for attenuation correction and anatomic reference were performed at 2, 4, and 7 days after injection with a Biograph mCT 64-slice PET/CT camera (Siemens).

As often, an additional dose of unlabeled antibody was required for imaging to guarantee sufficient circulating labeled antibody and thereby to improve tumor visualization (23, 26, 29, 32). We first verified the tracer biodistribution with escalating doses of 10, 50, and 100 mg of unlabeled lumretuzumab. We considered the unlabeled antibody dose to be sufficient when the circulation was adequately visualized 7 days after tracer injection. The optimal time point for PET scanning was determined by analyzing tumor tracer uptake serially at 2, 4, and 7 days after injection and available amount of tracer in the circulation.

In part B, patients underwent two series of ^{89}Zr-lumretuzumab PET imaging. The first series (baseline) was performed using the optimal imaging dose and schedule determined in part A ($\sim$1 mg ^{89}Zr-lumretuzumab along with 100-mg unlabeled lumretuzumab followed by PET scans at days 4 and 7 after injection). Fourteen days after the first tracer injection, a second tracer injection was administered and imaging repeated at optimal schedule. During the second series (on-treatment), ^{89}Zr-lumretuzumab was dosed with increasing PD-active doses of unlabeled lumretuzumab (400, 800, or 1,600 mg) in subsequent patient cohorts. These lumretuzumab doses had been cleared for safety in the phase I study, and all resulted in a downregulation of membranous HER3 protein measured by IHC in 35 of 38 tumor and skin biopsies 14 days after the first lumretuzumab administration compared with baseline (11).

After the last PET scan, patients continued with lumretuzumab monotherapy on a 2-weekly schedule and at the highest safe dose determined in the phase I study. Diagnostic CT scans were performed within 28 days before the first tracer injection and every 8 weeks ($\pm$7 days) after start of lumretuzumab treatment or if clinically indicated.

^{89}Zr-lumretuzumab PET analysis

PET scans were reconstructed (iterative reconstruction method: 28 matrix, two iterations, eight subsets, and 10-mm filter) and analyzed by a single dedicated nuclear medicine physician. All tumor lesions on the baseline diagnostic CT scan were recorded, including measurability according to RECIST 1.1 (33). Tumor lesions with visible tracer uptake on the ^{89}Zr-lumretuzumab PET were considered quantifiable when the tumor size was at least 10 mm, and measurement of tumor tracer uptake was considered not to be influenced by surrounding tissue (e.g., by the aorta or the liver). With the AMIDE (A Medical Image Data Examiner) software (version 0.9.3, Stanford University), radioactivity was quantified by manually drawing three dimensional volumes of interest (VOI) around tumor lesions and in the left ventricle (reflecting blood pool), liver, spleen, kidney, intestine, lung, brain, compact bone, and muscle to assess ^{89}Zr-lumretuzumab normal organ distribution (34). Standardized uptake values (SUVs) were calculated using the amount of injected activity, bodyweight, and the amount of radioactivity within a VOI. We report the SUVmax (the maximum voxel intensity in the VOI) for tumor lesions and SUVmean (the mean voxel intensity of all voxels in the VOI) for normal organ tracer uptake. Furthermore, the tumor-to-blood ratio (TBR) was calculated for all tumor lesions. In part B, baseline tumor tracer uptake, assessed during the first PET imaging series, was compared with tumor tracer uptake after the PD-active lumretuzumab dose during the second PET imaging series. In both series, the tumor tracer uptake was calculated as TBR to increase comparability, and the change in TBR with escalating PD-active doses of lumretuzumab served as a read out for target saturation.

In addition, the liver was delineated on all PET scans, and its volume and the radioactivity present were calculated. The activity of the liver was compared with the injected dose and the remaining dose in the body (VOI: head to tuber ischiadicum) on the respective PET scan and expressed as percent of injected (%ID) and percent of remaining dose (%RD), respectively.

Safety assessments

The National Cancer Institute Common Terminology Criteria for Adverse Events version 4.03 were used to evaluate side effects (35). Patients were assessed for adverse events at each clinical visit and if necessary throughout the study.

PK assessments

Blood samples were collected for determination of labeled and free ^{89}Zr and lumretuzumab PK before, directly after, as well as 2 and 4 hours following tracer injection and on the days of PET scans (2, 4, and 7 days after tracer injection) during the baseline scan series (parts A and B). After the second tracer injection (part B only), blood samples only for lumretuzumab PK were collected before, directly after, 2, 5 hours and 2, 4, and 7 days after injection.

Lumretuzumab concentration (in μg/mL) was determined in human serum using a validated ELISA method. Biotinylated ectodomain of human HER3, lumretuzumab reference standard or diluted samples, and anti-lumretuzumab detection antibody labeled with digoxigenin were bound to streptavidin-coated plates. The immobilized immune complexes were detected by anti-digoxigenin antibody conjugated to horseradish peroxidase. 3,3′,5,5′-Tetramethylbenzidine substrate was used to produce a colorimetric signal photometrically determined at 450 nm (690 nm reference wave length) which is proportional to the lumretuzumab amount in the sample. The calibration was 10.0 to 1,000 ng/mL for lumretuzumab in 100% human serum. The lower limit of quantification was 15.0 ng/mL in native human serum.

Activity (in counts per minute) of ^{89}Zr was measured in 1 mL serum and in 1 mL whole blood using a calibrated well-type γ-counter (LKB Instruments), followed by conversion to radioactivity concentration (Bq/mL). The radioactivity concentrations of serum and whole blood samples were then compared with the activity in the blood pool (Bq/mL) on PET scans, and to the measured lumretuzumab serum concentrations.

Statistical analyses

Statistical analyses were performed using SPSS Version 22. Significant differences between two groups were calculated either using independent sample Student *t*-test or Mann–Whitney U test depending on normality of distribution as assessed by the Shapiro–Wilk test. In case of three or more groups with normally distributed data, significant differences were calculated using a one-way ANOVA with either *posthoc* Gabriel or Games–Howell test depending on homogeneity of variances as assessed by Levene test. If data were not normally distributed, groups were compared using a Kruskal–Wallis followed by a Mann–Whitney *U* test. $P \leq 0.05$ was considered to be a significant difference. All analyses were two-sided. Bivariate correlations were performed using Pearson (for continuous variables) or Spearman (for ordinal variables) correlation coefficients. Data are presented as mean $\pm$ SD, unless otherwise stated.

Results

Patient characteristics

Twenty patients were enrolled from December 2012 until November 2014, 7 in part A and 13 in part B. Patient characteristics are summarized in Table 1 and Supplementary Fig. S1.

Eighteen of 20 patients received one or more infusions of lumretuzumab (range, 0–8; median, 4) after baseline ^{89}Zr-lumretuzumab PET.

^{89}Zr-lumretuzumab PET

Optimal imaging dose and schedule. The optimal imaging dose was assessed in seven patients across three cohorts. Patients in the first two cohorts ($n = 2$ each) received approximately 1 mg ^{89}Zr-lumretuzumab with either 10 or 50 mg additional unlabeled lumretuzumab. At both doses, the amount of tracer left in the circulation 7 days after injection was too low for adequate tumor visualization (SUVmean in blood 7 days after injection 0.5 ± 0.2 with 10 mg, 2.3 ± 1.5 with 50-mg unlabeled lumretuzumab). Therefore, another three patients received ^{89}Zr-lumretuzumab together with 100 mg of unlabeled lumretuzumab, which resulted in sufficient tracer present in the circulation 7 days after injection (SUVmean in blood of 3.6 ± 1.1) to allow adequate tumor visualization. Improved blood tracer availability over time resulted in superior imaging results compared with the 10 and 50-mg dose cohorts. Mean tumor tracer uptake increased from SUVmax 1.8 ± 1.1 assessed in 25 tumor lesions (10 mg) to 4.2 ± 2.4 assessed in 18 lesions (100 mg; $P < 0.05$). The PET scan 2 days after injection was omitted in part B, as it did not add information to the PET scans performed 4 and 7 days after injection.

Organ distribution. Normal organ distribution was evaluated in all 16 patients who received 100-mg unlabeled lumretuzumab together with the tracer followed by at least two baseline PET scans 4 and 7 days after injection (part A $n = 3$, part B $n = 13$). On day 4 after injection, the highest tracer uptake was seen in the liver with SUVmean of 6.4 ± 1.1 (Fig. 1). Furthermore, relatively high tracer levels were seen in the circulation (4.9 ± 1.3), the kidneys (4.2 ± 0.8), spleen (3.8 ± 1.1), and intestine (3.1 ± 1.2). Tracer uptake was much lower in brain, muscle, bone, abdominal cavity, and lung (SUVmean 0.2 ± 0.1, 0.5 ± 0.2, 0.6 ± 0.2, 0.6 ± 0.3, and 0.9 ± 0.2, respectively). Comparable tracer distributions were seen on day 7 after injection, and in the patients who received 10- or 50-mg unlabeled lumretuzumab in part A.

Relatively high tracer uptake was observed in healthy liver tissue, which was comparable across dose levels at baseline and after the first lumretuzumab dose ($P > 0.05$; Fig. 1 and Supplementary Fig. S2). When compared with injected imaging dose, liver uptake decreased over time from 10.2 %ID (±2.7) on day 2 to 3.4 %ID (±2.9) on day 7 (Supplementary Fig. S2A) during the baseline scan series and was comparable after the first PD-active dose ($P > 0.05$). After correcting for the amount of radioactivity remaining in the body assessed on the PET scan, the liver uptake for all dose cohorts did not differ ($P > 0.05$) with a mean liver

Table 1. Patient characteristics

Characteristic	All patients ($n = 20$)
Age, median years (range)	62.5 (45–72)
Sex	
Male, *n* (%)	10 (50)
Female, *n* (%)	10 (50)
ECOG PS	
0, *n* (%)	12 (60)
1, *n* (%)	5 (25)
2, *n* (%)	3 (15)
Tumor type, *n* (%)	
Rectal cancer	7 (35)
Colon cancer	4 (20)
Head and neck cancer	2 (10)
Cancer of unknown primary[a]	2 (10)
Ovarian cancer	1 (5)
Esophageal cancer	1 (5)
Breast cancer	1 (5)
Cancer of the ampulla of Vater	1 (5)
Vulvar cancer	1 (5)
Prior systemic palliative therapies, *n*	
0	5 (25)
1	3 (15)
2	4 (20)
>2 (3–7)	8 (40)

[a]Tumor cells were considered of epithelial origin based on positive staining of at least one epithelial marker (cytokeratins, EMA, and EpCAM).

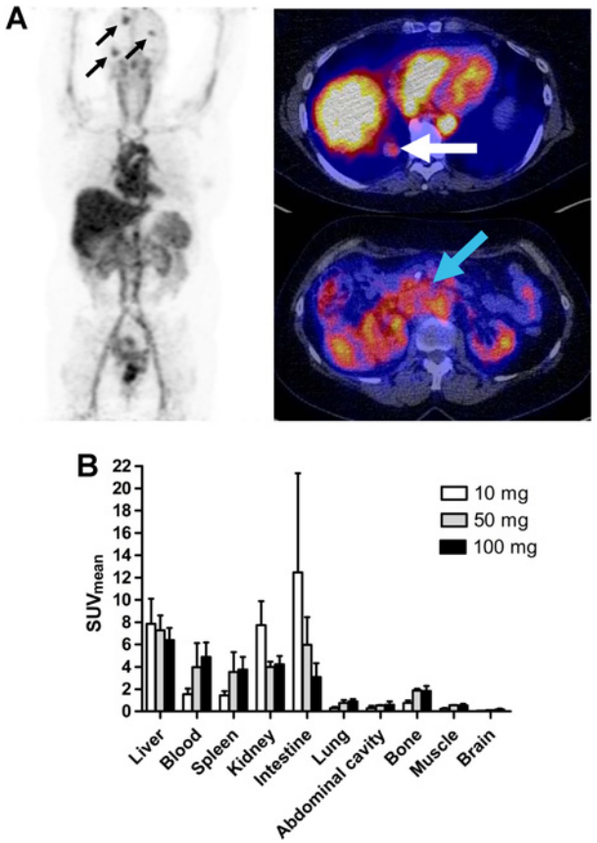

Figure 1.
A, ^{89}Zr-lumretuzumab PET scan with 100-mg unlabeled lumretuzumab 4 days after injection with representative whole body tracer distribution and tracer uptake in multiple brain metastases (black arrows), one lung metastasis behind the liver (white arrow), and the primary tumor (cancer of the ampulla of Vater, blue arrow). **B,** ^{89}Zr-lumretuzumab organ biodistribution 4 days after injection for different doses of unlabeled lumretuzumab; 10-mg unlabeled lumretuzumab in white bars ($n = 2$), 50-mg unlabeled lumretuzumab in gray bars ($n = 2$), 100-mg unlabeled lumretuzumab in black bars ($n = 16$).

uptake of 14.6% (±0.8) of the remaining dose (%RD; Supplementary Fig. S2B).

Tracer uptake in tumor lesions. Overall, a total of 598 tumor lesions (median number of lesions per patient: 18; range, 3–159) from 20 patients were recorded based on the diagnostic CT scans (Supplementary Table S1). Of these, 382 lesions were <10 mm. Of the 216 lesions ≥10 mm, 146 lesions (67.6%) were visible on ^{89}Zr-lumretuzumab PET, of which 115 (53.2%) had quantifiable ^{89}Zr-lumretuzumab tracer uptake. In all but one patient, tracer uptake was observed in at least one lesion. A median of 5 (range, 0–20) lesions per patient were quantifiable for ^{89}Zr-lumretuzumab tracer uptake. Seventy of the 216 lesions (32.4%) with a diameter ≥10 mm were not visible on ^{89}Zr-lumretuzumab PET. Of these 70 lesions, 19 were liver metastases where visible tracer uptake was precluded by the relatively higher tracer uptake of surrounding normal liver tissue. The remaining 51 nonvisible lesions in 17 patients were located outside the liver.

Using 10 mg of unlabeled lumretuzumab SUVmax was 2.7 (±1.1), 2.2 (±1.0), and 1.8 (±1.1) in 25 quantifiable tumor lesions in two patients on 2, 4, and 7 days after injection, respectively. At 50 mg, SUVmax was comparable ($n = 2$ patients with 13 lesions). At 100 mg of unlabeled lumretuzumab, SUVmax increased to 4.0 (±2.1) 2 days after injection ($n = 3$ patients with 18 lesions, part A), 3.4 (±1.9) 4 days after injection, and 3.4 (±2.1) 7 days after injection (both 4 and 7 days after injection; $n =$ 16 patients with 77 lesions, parts A and B) and the TBR increased over time (Supplementary Fig. S3). The highest SUVmax at the 100-mg dose level was seen in eight abdominal lesions (adrenal gland, intestine and ovaries, and other unspecified abdominal tissue lesions) with 6.0 (±1.9) and 6.0 (±2.2) 4 and 7 days after injection, respectively (Table 2). Furthermore, tumor uptake was also high in head and neck lesions, lymph nodes, brain lesions, and a previously unknown bone metastasis, but lower in pulmonary and subcutaneous lesions. Ascites and/or pleural effusion present in three patients were also visible on all PET scans.

^{89}Zr-lumretuzumab tracer uptake was shown in at least one tumor lesion in 19 of 20 patients. In the patient without tumor tracer uptake, all five lesions visible on the CT scan were located in the liver. Here, ^{89}Zr-lumretuzumab uptake was lower than in the surrounding liver tissue and therefore not reliably quantifiable (Fig. 2).

Table 2. ^{89}Zr-lumretuzumab tumor uptake at the 100-mg unlabeled lumretuzumab dose level

Tumor lesion, organ (*n*)	SUVmax (SD) 4 days pi	SUVmax (SD) 7 days pi
Solid quantifiable lesions[a] (77)		
Abdominal lesions[b] (8)	6.0 (1.9)	6.0 (2.2)
Lymph node (11)	5.1 (1.4)	4.8 (1.9)
Head and neck (4)	4.9 (0.9)	3.8 (0.9)
Bone[c] (1)	4.5	5.4
Brain (5)	3.9 (1.7)	4.9 (2.1)
Lung (43)	2.4 (1.2)	2.4 (1.5)
Subcutaneous lesion (5)	2.1 (0.4)	1.9 (0.3)
Malignant fluids[d] (5)		
Ascites (2)	6.4 (0.4)	5.4 (3.)
Pleural effusion (3)	3.0 (1.6)	2.6 (1.1)

Abbreviation: pi, postinjection.
[a]Seventy-seven lesions assessed in 16 patients who received 100-mg unlabeled lumretuzumab in addition to the tracer.
[b]Abdominal lesions include lesions in the adrenal gland, the intestine, ovaries, and other unspecified abdominal tissue.
[c]The detected bone metastases were previously unknown and confirmed by MRI after the ^{89}Zr-lumretuzumab PET.
[d]Malignant fluids were found in three patients, one having both ascites and pleural effusion.

Tumor ^{89}Zr-lumretuzumab tracer uptake after the first PD-active dose of lumretuzumab compared with baseline. Fourteen days after the first tracer injection (~1 mg ^{89}Zr-lumretuzumab together with 100-mg unlabeled lumretuzumab), patients in part B ($n = 13$) received a second tracer injection with 400-, 800-, or 1,600-mg lumretuzumab followed by a scan 4 and 7 days after injection to evaluate the decrease in tracer uptake and potential target saturation. Differences in tracer uptake were evaluable in seven of the 13 patients. In the remaining six patients, this failed due to the absence of tumor lesions (repeatedly) quantifiable for tracer uptake ($n = 2$), obesity (body mass index of 45 in one patient), high liver uptake during the second scan series exceeding baseline liver uptake influencing normal tracer biodistribution ($n = 1$), technical problems ($n = 1$), and no second series due to progressive disease ($n = 1$).

Six lesions in the 400-mg cohort, nine lesions in the 800-mg cohort, and eight lesions in the 1,600-mg cohort were quantifiable (Supplementary Table S2). A decrease in tumor tracer uptake at day 4 after the first PD-active dose and the corresponding baseline PET was seen in all six lesions at the 400-mg dose level, in six of

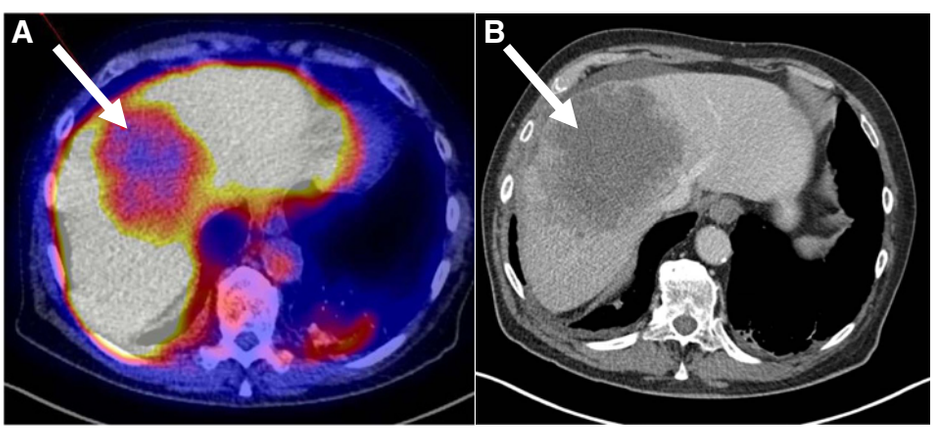

Figure 2.
^{89}Zr-lumretuzumab PET (**A**) and diagnostic CT scan (**B**) of the liver of patient 4. The liver metastasis (white arrow) is visually cold on the ^{89}Zr-lumretuzumab PET scan 7 days after injection of the tracer with additional 50-mg unlabeled lumretuzumab.

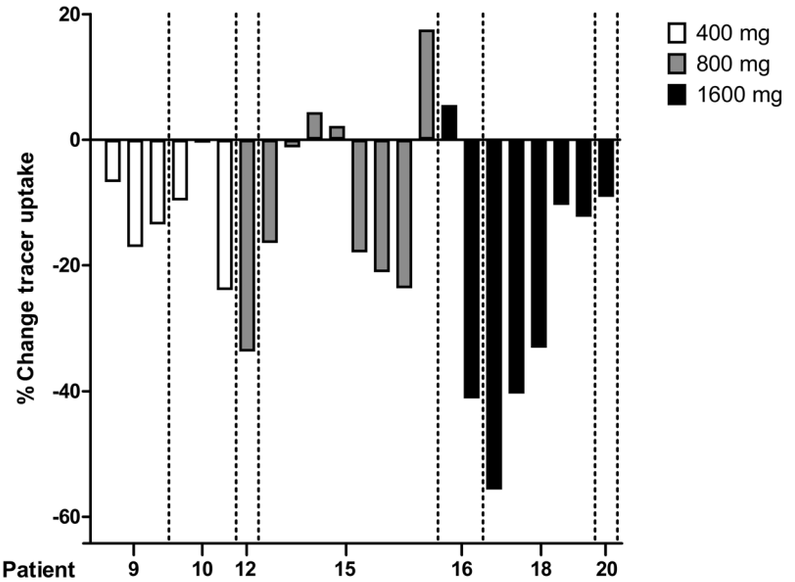

Figure 3.
Percentage change of tracer uptake (as tumor-to-blood ratio) after the first PD-active dose of lumretuzumab (400, 800, or 1,600 mg) versus baseline (100-mg unlabeled lumretuzumab) in 23 quantifiable lesions ($n = 7$ patients) 4 days after injection.

nine lesions at 800 mg, and in seven of eight lesions at 1,600 mg (Fig. 3 and Supplementary Table S3). In the 800-mg cohort, the three lesions without a decrease in tracer uptake were located in the lung, whereas the one at 1,600 mg without a decrease in uptake was an abdominal lesion.

The tumor tracer uptake (as percentage change in TBR) in the quantifiable lesions decreased 4 days after injection by 11.9% (±8.2%) at 400 mg, 10.0% (±16.5%) at 800 mg, and 24.6% (±20.9%) at 1,600 mg compared with the baseline PET scan with 100 mg of unlabeled lumretuzumab, whereas at 7 days after injection, the decrease in tumor uptake was 1.5% (±14.0%) at 400 mg, 16.9% (±12.4%) at 800 mg, and 11.8% (±28.2%) at 1,600 mg compared with baseline (Supplementary Fig. S4).

Lumretuzumab and ^{89}Zr PK

The PK of lumretuzumab was nonlinear from 10 mg up to 100 mg. Both C_{max} and AUC_{last} showed a greater than dose proportional increase, accompanied by a decline in clearance over the same dose range, indicating that the elimination of lumretuzumab across this dose range was predominantly target-mediated. Overall, systemic exposure (AUC_{last}) during the first cycle in patients treated with 400, 800, and 1,600 mg increased dose proportional with comparable total clearance. PK variability was observed among cohorts and within cohorts.

Activity of ^{89}Zr assessed in serum and whole blood samples and lumretuzumab serum concentration correlated strongly with blood pool activity assessed on PET scans at baseline (Supplementary Fig. S5).

HER3 expression

HER3 tumor expression was seen in all 20 patients at baseline (Supplementary Fig. S6). In 11 of 12 biopsied nonhepatic tumor lesions, tracer uptake was visible on ^{89}Zr-lumretuzumab PET. The one metastasis without visible tracer uptake was an abdominal lesion. Tracer uptake at either day 4 or day 7 did not correlate with baseline HER3 tumor expression [Spearman correlation coefficient = 0.049 ($P = 0.89$) and 0.049 ($P = 0.89$), respectively, $n = 10$; Table 3].

Membranous HER3, assessed in paired skin biopsies ($n = 8$ patients in part B), was completely downregulated 14 days after the first PD-active lumretuzumab dose compared with baseline (HER3 IHC as median IRS: pre 0.69, post 0; $P < 0.0001$), which is in line with previously published data (11).

Efficacy and safety of lumretuzumab monotherapy

After the baseline ^{89}Zr-lumretuzumab PET scans, the first patient in part A received lumretuzumab at a dose of 1,600 mg for further treatment. All following patients received 2,000-mg lumretuzumab. Patients received lumretuzumab for a median of four cycles (range, 0–8 cycles) or a median duration of 57 days (range, 1–120 days). Five patients (25%) had as best response stable disease. Patients were discontinued from the study due to progressive disease according to RECIST 1.1 ($n = 17$), clinical progression ($n = 2$), or death ($n = 1$).

Baseline ^{89}Zr-lumretuzumab tracer uptake in individual target lesions did not correlate with size change on CT during first or second response assessment ($n = 14$ patients with 31 lesions and $n = 4$ patients with six lesions, respectively).

The ^{89}Zr-lumretuzumab tracer and lumretuzumab monotherapy up to 2000 mg per cycle were well tolerated (Supplementary Table S4).

Discussion

In this study, we were able to characterize the biodistribution of ^{89}Zr-lumretuzumab and tumor uptake by serial imaging with the ^{89}Zr-labeled therapeutic antibody lumretuzumab before and during treatment in patients with advanced or metastatic HER3-positive solid tumors. Although PD-active lumretuzumab doses decreased ^{89}Zr-lumretuzumab uptake, there was no clear evidence of tumor saturation by PET imaging as the tumor SUV did not plateau with increasing doses.

Development of therapeutic HER3 antibodies is still in an early phase. Results of first trials with these HER3 antibodies indicate that further application of these drugs will focus on biomarker-enriched populations, as well as on combination

Table 3. Tumor HER3 expression and ^{89}Zr-lumretuzumab tumor tracer uptake

Patient	Unlabeled lumretuzumab (mg)	Tumor lesion, organ	HER3 expression (IRS)	^{89}Zr-lumretuzumab uptake (SUVmax)	
				4 days pi	7 days pi
1[a]	10	Lung	2.90	2.37	1.52
2	10	Lymph node	2.90	-[b]	-[b]
3	50	Lung	1.62	2.12	2.29
4[a]	50	Liver[c]	2.50	-	-
5[a]	100	Lung	0.078	2.39	1.86
6	100	Subcutaneous lesion	2.40	2.29	2.14
7[a]	100	Liver[c]	2.25	-	-
8	100	Liver[c]	2.50	-	-
9	100	Head and neck	1.35	5.98	4.89
10	100	Liver[c]	0.0035	-	-
11	100	Head and neck	0.16	5.63	3.89
12	100	Liver[c]	2.43	-	-
13	100	Lung	1.71	1.65	1.64
14[a]	100	Liver[c]	2.57	-	-
15	100	Lung	2.71	3.88	4.23
16	100	Abdominal lesion[d]	3.0	7.93	7.54
17[a]	100	Abdominal lesion[d,e]	1.62	2.14[e]	2.35[e]
18[a]	100	Liver[c]	1.13	-	-
19	100	Liver[c]	2.25	-	-
20	100	Ascites[f]	NA	6.68	7.75

Abbreviations: IRS, immunoreactive score; NA, not available; pi, postinjection.
[a]Patients who received EGFR-targeted therapy in any line prior to inclusion in this study.
[b]Lesion was visible on ^{89}Zr-lumretuzumab PET, but tracer uptake was not reliably quantifiable due to adjacent vessels with high blood activity.
[c]Tracer uptake in hepatic lesions is not visible and not quantifiable on ^{89}Zr-lumretuzumab PET due to high tracer uptake of surrounding normal liver tissue.
[d]Abdominal lesions include metastasis in the intestine and ovaries.
[e]The abdominal mass of patient 17 was visually negative on ^{89}Zr-lumretuzumab PET, the lesion was quantified for correlation analysis.
[f]For IHC, tumor cells were obtained from malignant cell–rich ascites.

with other treatments targeting other HER family members (11). This makes insight in biodistribution, information on intra- and interpatient target heterogeneity and target accessibility, as well as target occupation or even saturation of utmost importance. First attempts to label an HER3 antibody were made in a small study with Copper-64-tetra-azacyclododecanetetra-acetic acid (^{64}Cu-DOTA)-patritumab, and feasibility was shown (36). We preferred ^{89}Zr over ^{64}Cu as its longer half-life of 78.4 hours compared with 12.7 hours for ^{64}Cu better matches the half-life of lumretuzumab (30, 37). Furthermore, the target saturation for different PD-active doses of lumretuzumab was analyzed in the current study.

All but one patient, who had liver metastases only, showed quantifiable tracer tumor uptake in at least one metastasis. Tumor uptake of ^{89}Zr-lumretuzumab varied within and between patients, with tumor SUVmax ranging from 0.5 up to 8.9 with up to a sixfold difference in mean tumor tracer uptake between patients. Lesions with a diameter $\geq$ 10 mm were ^{89}Zr-lumretuzumab PET-negative in 32.4%. Although testing positive for HER3 by IHC, the PET-negative lesions and the observed variance in ^{89}Zr-lumretuzumab tumor uptake may be a result of intratumor and intrapatient target heterogeneity. In addition, it may well be that lesions with low tracer uptake or PET-negative lesions have other characteristics than PET-positive lesions causing lack of tracer permeability within those lesions. Contributing factors might be the vascularization, tissue permeability and retention, as well as the size of the lesion (38). These factors together with low target expression could have generated insufficient signal to be picked up adequately by PET imaging on the late scan moments with the used scan time and administered dose of radioactivity.

Similar results on heterogeneity of tumor tracer uptake were reported for the ZEPHIR trial, where one-third of patients with HER2-positive metastatic breast cancer were considered ^{89}Zr-trastuzumab PET-negative before start of treatment with trastuzumab-emtansine (39). Another trial assessing the biodistribution and PD of the Indium-111–labeled, anti-human death receptor 5 (DR5) monoclonal antibody tigatuzumab, seven of 19 patients (37%) with metastatic colorectal cancer also had no SPECT-positive lesions and tumor tracer uptake did not correlate with DR5 expression or tumor response (40). In both trials, target heterogeneity and tissue-dependent properties were proposed factors to influence general tracer availability and tumor tracer uptake. To conclude, all these studies suggest that we most likely underestimate other factors which may influence penetration of drugs and local drug concentration in the tumor, next to heterogeneity in target expression.

^{89}Zr-lumretuzumab uptake in liver metastases was always considered negative on PET imaging given relatively higher ^{89}Zr-lumretuzumab background activity in healthy liver tissue. The background liver tracer uptake even exceeded tumor lesions with the highest uptake outside the liver. This is clearly different from ^{89}Zr-trastuzumab uptake in liver metastases, which was almost twofold higher compared with surrounding healthy liver tissue in patients with HER2-positive metastatic breast cancer (23). The high tracer accumulation in healthy liver tissue might be due to uptake and metabolism of (^{89}Zr-labeled) lumretuzumab by healthy liver nonparenchymal Kupffer cells due to glycosylation of lumretuzumab. Especially glycosylation with mannose increases blood clearance of the antibody and enhances antibody-dependent cell-mediated cytotoxicity (ADCC) against tumor cells (41). As the liver is a key organ in antibody clearance and attracting the immune system for ADCC, it might explain the relatively higher tracer uptake in healthy liver tissue compared with liver metastases. This, however, did not result in specific liver toxicity or higher efficacy in liver metastases (11). On the other hand, the target receptor density, which is generally lower in

HER3-positive tumor lesions compared with HER2-positive lesions, might also explain the PET-negative liver lesions.

For optimal imaging results, an additional dose of 100 mg of unlabeled lumretuzumab was required, as lower doses did not result in sufficient tracer in the circulation for adequate tumor visualization. For imaging of a number of antibodies without dose-dependent PK, such as bevacizumab, fresolizumab, or the mesothelin-targeting antibody MMOT0530A, a dose of 5- or 10-mg unlabeled antibody was already sufficient for optimal PET imaging (24, 29, 32, 42). However, for HER2 imaging with ^{89}Zr-trastuzumab, an antibody with clear dose-dependent PK, an additional dose of 50 mg unlabeled trastuzumab is needed for optimal imaging (43, 44). As described previously, we showed that lumretuzumab has also dose-dependent PK with declining clearance up to 400-mg dose, which at least in part explains the need of additional 100-mg unlabeled antibody for optimal imaging (11).

The organ biodistribution of ^{89}Zr-lumretuzumab was largely comparable with the distribution of other ^{89}Zr-labeled antibodies (23–25). The highest uptake was observed in the liver (14.6% of the remaining dose) and intestine, representing locations of antibody metabolism and excretion without showing clear signs of organ-specific drug-mediated toxicity.

In the absence of side effects, therapeutic antibodies may easily be dosed above the maximum tumor saturation (45). In this study, there was a dose proportional increase of systemic exposure from 400-mg to 1,600-mg lumretuzumab. A decrease in tumor tracer uptake between PET assessments after administration of the first PD-active dose compared with baseline was detectable. The decrease in tumor tracer uptake at 4 days after injection compared with baseline was the highest at the highest tested lumretuzumab dose of 1,600 mg, confirming PD activity but without showing a plateau. Immunohistochemical analyses of skin samples showed receptor saturation at and above lumretuzumab doses of 400 mg 14 days following the first PD-active dose. Regretfully, the resolution of PET does not allow visualizing the skin as a separate organ and therefore precludes comparison with tumor saturation. Furthermore, we performed PET imaging only up to 7 days after the first PD-active lumretuzumab administration, which might have been too early to visualize the full effect of the dose.

Based on assumptions from classic saturation analysis, the dose at which no additional decrease in tumor drug uptake is seen would confirm target saturation and would identify the maximum required drug dose (46). However, receptor expression and related processes are dynamic and novel ways of analysis might be helpful to take receptor dynamics into account. From preclinical assessments, it is known that HER3 membrane expression is highly dynamic and expression is influenced by internalization, degradation, and relocation to the membrane of formerly internalized receptors (47). Furthermore, internalization might even be increased by activation of endocytosis due to antibody treatment further increasing receptor internalization (48–50). With molecular imaging of ^{89}Zr-tracers, more than with other techniques, such dynamic processes might influence the outcome. Thereby, PET visualizes a combination of membrane-bound activity, as well as the intracellular fraction as the relatively long-living radionuclide ^{89}Zr residualizes in tumor cells after internalization. This information differs from the HER3 expression measured serially in (skin) biopsies in this trial by scoring membrane staining only (37). Other factors influencing tumor tracer uptake might be the effect of enhanced permeability and retention in tumor lesions and (unspecific) tracer uptake, for example, due to the effect of Fc gamma receptor engagement within the tumor environment possibly differing between tumor types. To correct for variance in tracer blood levels, the tumor-to-blood ratios were used to assess the difference in uptake after administration of the PD-active dose and baseline imaging. Furthermore, in patients with HER2-positive breast cancer, ^{111}In-trastuzumab scintigraphy showed a decrease in tumor uptake of only 20% during steady state following three therapeutic doses of trastuzumab (42). Data from this and our trial might also suggest that it might be impossible to completely saturate these receptors due to its constant renewal and relocation. To obtain additional insight in tracer accumulation and behavior on a cellular level, however, additional microscopic fluorescence imaging using fluorescent tracers might be considered in future trials. Furthermore, when HER3 antibodies get a firmer place in the clinic, a broader role for this tracer including assessment of the ability to predict tumor response to treatment can be foreseen.

In conclusion, we demonstrated ^{89}Zr-lumretuzumab biodistribution and specific tumor tracer uptake in patients with HER3-positive epithelial tumors and observed inter- and intrapatient heterogeneity in lesions across the body apart from the liver. Serial imaging after the first PD-active dose with HER3 downregulation in skin biopsies at and above 400-mg lumretuzumab showed reduced tumor tracer uptake compared with baseline, confirming PD activity. In contrast to the phase I PD data, there was no clear evidence of tumor saturation by PET imaging as the tumor SUV did not plateau with increasing doses. This suggests highly dynamic receptor processes, but could also be influenced by technical limitations, variable expression levels of the target, as well as variable saturation kinetics.

Disclosure of Potential Conflicts of Interest

W. Jacob holds ownership interest (including patents) in Roche stock. M. Weisser holds ownership interest (including patents) in Roche shares. No potential conflicts of interest were disclosed by the other authors.

Authors' Contributions

Conception and design: F. Bensch, L.E. Lamberts, M.N. Lub-de Hooge, A.G.T. Terwisscha van Scheltinga, M. Thomas, W. Jacob, K. Abiraj, G. Meneses-Lorente, M. Weisser, E.G.E. de Vries

Development of methodology: L.E. Lamberts, A. Jorritsma-Smit, M.N. Lub-de Hooge, A.G.T. Terwisscha van Scheltinga, J.R. de Jong, A.H. Brouwers, E.G.E. de Vries

Acquisition of data (provided animals, acquired and managed patients, provided facilities, etc.): F. Bensch, L.E. Lamberts, M.M. Smeenk, M.N. Lub-de Hooge, C.P. Schröder, M. Thomas, A.H. Brouwers, E.G.E. de Vries

Analysis and interpretation of data (e.g., statistical analysis, biostatistics, computational analysis): F. Bensch, L.E. Lamberts, M.M. Smeenk, A.G.T. Terwisscha van Scheltinga, J.R. de Jong, C.P. Schröder, M. Thomas, W. Jacob, K. Abiraj, G. Meneses-Lorente, I. James, M. Weisser, A.H. Brouwers, E.G.E. de Vries

Writing, review, and/or revision of the manuscript: F. Bensch, L.E. Lamberts, M.M. Smeenk, M.N. Lub-de Hooge, A.G.T. Terwisscha van Scheltinga, J.R. de Jong, J.A. Gietema, C.P. Schröder, M. Thomas, W. Jacob, K. Abiraj, C. Adessi, G. Meneses-Lorente, I. James, M. Weisser, A.H. Brouwers, E.G.E. de Vries

Administrative, technical, or material support (i.e., reporting or organizing data, constructing databases): F. Bensch, L.E. Lamberts, M.M. Smeenk, M.N. Lub-de Hooge, I. James

Study supervision: J.A. Gietema, M. Weisser, A.H. Brouwers, E.G.E. de Vries

Other (pharmacovigilance activities): C. Adessi

Acknowledgments

We thank Linda Pot and Rianne Bakker for technical support for the labeling procedures and Paul van Snick, Johan Wiegers, and Eelco Severs for their assistance with PET data transfer.

Grant Support

The ERC-advanced grant OnQview was provided to E.G.E. de Vries, and financial support for the study was provided by F. Hoffmann–La Roche Ltd to the UMCG.

The costs of publication of this article were defrayed in part by the payment of page charges. This article must therefore be hereby marked *advertisement* in accordance with 18 U.S.C. Section 1734 solely to indicate this fact.

Received February 3, 2017; revised May 30, 2017; accepted July 18, 2017; published OnlineFirst July 21, 2017.

References

1. Campbell MR, Amin D, Moasser MM. HER3 comes of age: new insights into its functions and role in signaling, tumor biology, and cancer therapy. Clin Cancer Res 2010;16:1373–83.
2. Prigent SA, Lemoine NR, Hughes CM, Plowman GD, Selden C, Gullick WJ. Expression of the c-erbB-3 protein in normal human adult and fetal tissues. Oncogene 1992;7:1273–8.
3. Hayashi M, Inokuchi M, Takagi Y, Yamada H, Kojima K, Kumagai J, et al. High expression of HER3 is associated with a decreased survival in gastric cancer. Clin Cancer Res 2008;14:7843–9.
4. Cao GD, Chen K, Xiong MM, Chen B. HER3, but not HER4, plays an essential role in the clinicopathology and prognosis of gastric cancer: a meta-analysis. PLoS One 2016;11:e0161219.
5. Debska-Szmich S, Kusinska R, Czernek U, Szydlowska-Pazera K, Habib-Lisik M, Piekarski JH, et al. Prognostic value of HER3, PTEN and p-HER2 expression in patients with HER2-positive breast cancer. Postepy Hig Med Dosw 2015;69:586–97.
6. Tanner B, Hasenclever D, Stern K, Schormann W, Bezler M, Hermes M, et al. ErbB-3 predicts survival in ovarian cancer. J Clin Oncol 2006;24:4317–23.
7. Hirakawa T, Nakata B, Amano R, Kimura K, Shimizu S, Ohira G, et al. HER3 overexpression as an independent indicator of poor prognosis for patients with curatively resected pancreatic cancer. Oncology 2011;81:192–8.
8. Sithanandam G, Anderson LM. The ERBB3 receptor in cancer and cancer gene therapy. Cancer Gene Ther 2008;15:413–48.
9. Ocana A, Vera-Badillo F, Seruga B, Templeton A, Pandiella A, Amir E. HER3 overexpression and survival in solid tumors: a meta-analysis. J Natl Cancer Inst 2013;105:266–73.
10. Mirschberger C, Schiller CB, Schraml M, Dimoudis N, Friess T, Gerdes CA, et al. RG7116, a therapeutic antibody that binds the inactive HER3 receptor and is optimized for immune effector activation. Cancer Res 2013;73:5183–94.
11. Meulendijks D, Jacob W, Martinez-Garcia M, Taus A, Lolkema M, Voest E, et al. First-in-human phase I study of lumretuzumab, a glycoengineered humanized anti-HER3 monoclonal antibody, in patients with metastatic or advanced HER3-positive solid tumors. Clin Cancer Res 2016;22:877–85.
12. Burrell RA, Swanton C. Tumour heterogeneity and the evolution of polyclonal drug resistance. Mol Oncol 2014;8:1095–111.
13. Heitz F, Barinoff J, du Bois O, Hils R, Fisseler-Eckhoff A, Harter P, et al. Differences in the receptor status between primary and recurrent breast cancer-the frequency of and the reasons for discordance. Oncology 2013;84:319–25.
14. Moussa O, Purdie C, Vinnicombe S, Thompson AM. Biomarker discordance: prospective and retrospective evidence that biopsy of recurrent disease is of clinical utility. Cancer Biomark 2012;12:231–9.
15. Houssami N, Macaskill P, Balleine RL, Bilous M, Pegram MD. HER2 discordance between primary breast cancer and its paired metastasis: tumor biology or test artefact? Insights through meta-analysis. Breast Cancer Res Treat 2011;129:659–74.
16. Siyar Ekinci A, Demirci U, Cakmak Oksuzoglu B, Ozturk A, Esbah O, Ozatli T, et al. KRAS discordance between primary and metastatic tumor in patients with metastatic colorectal carcinoma. J BUON 2015;20:128–35.
17. Amir E, Ooi WS, Simmons C, Kahn H, Christakis M, Popovic S, et al. Discordance between receptor status in primary and metastatic breast cancer: an exploratory study of bone and bone marrow biopsies. Clin Oncol (R Coll Radiol) 2008;20:763–8.
18. Lower EE, Glass E, Blau R, Harman S. HER-2/neu expression in primary and metastatic breast cancer. Breast Cancer Res Treat 2009;113:301–6.
19. Curigliano G, Bagnardi V, Viale G, Fumagalli L, Rotmensz N, Aurilio G, et al. Should liver metastases of breast cancer be biopsied to improve treatment choice? Ann Oncol 2011;22:2227–33.
20. Tosi D, Laghzali Y, Vinches M, Alexandre M, Homicsko K, Fasolo A, et al. Clinical development strategies and outcomes in first-in-human trials of monoclonal antibodies. J Clin Oncol 2015;33:2158–65.
21. Lamberts LE, Williams SP, Terwisscha van Scheltinga AG, Lub-de Hooge MN, Schroder CP, Gietema JA, et al. Antibody positron emission tomography imaging in anticancer drug development. J Clin Oncol 2015;33:1491–504.
22. Van Dongen GA, Poot AJ, Vugts DJ. PET imaging with radiolabeled antibodies and tyrosine kinase inhibitors: immuno-PET and TKI-PET. Tumour Biol 2012;33:607–15.
23. Dijkers EC, Oude Munnink TH, Kosterink JG, Brouwers AH, Jager PL, de Jong JR, et al. Biodistribution of ^{89}Zr-trastuzumab and PET imaging of HER2-positive lesions in patients with metastatic breast cancer. Clin Pharmacol Ther 2010;87:586–92.
24. Oosting SF, Brouwers AH, van Es SC, Nagengast WB, Oude Munnink TH, Lub-de Hooge MN, et al. ^{89}Zr-bevacizumab PET visualizes heterogeneous tracer accumulation in tumor lesions of renal cell carcinoma patients and differential effects of antiangiogenic treatment. J Nucl Med 2015;56:63–9.
25. Gaykema SB, Brouwers AH, Lub-de Hooge MN, Pleijhuis RG, Timmer-Bosscha H, Pot L, et al. ^{89}Zr-bevacizumab PET imaging in primary breast cancer. J Nucl Med 2013;54:1014–8.
26. Gaykema SB, Schroder CP, Vitfell-Rasmussen J, Chua S, Oude Munnink TH, Brouwers AH, et al. ^{89}Zr-trastuzumab and ^{89}Zr-bevacizumab PET to evaluate the effect of the HSP90 inhibitor NVP-AUY922 in metastatic breast cancer patients. Clin Cancer Res 2014;20:3945–54.
27. Borjesson PK, Jauw YW, Boellaard R, de Bree R, Comans EF, Roos JC, et al. Performance of immuno-positron emission tomography with zirconium-89-labeled chimeric monoclonal antibody U36 in the detection of lymph node metastases in head and neck cancer patients. Clin Cancer Res 2006;12:2133–40.
28. Rizvi SN, Visser OJ, Vosjan MJ, van Lingen A, Hoekstra OS, Zijlstra JM, et al. Biodistribution, radiation dosimetry and scouting of ^{90}Y-ibritumomab tiuxetan therapy in patients with relapsed B-cell non-Hodgkin's lymphoma using ^{89}Zr-ibritumomab tiuxetan and PET. Eur J Nucl Med Mol Imaging 2012;39:512–20.
29. Den Hollander MW, Bensch F, Glaudemans AW, Oude Munnink TH, Enting RH, den Dunnen WF, et al. TGF-β antibody uptake in recurrent high-grade glioma imaged with ^{89}Zr-fresolimumab PET. J Nucl Med 2015;56:1310–4.
30. Terwisscha van Scheltinga AG, Lub-de Hooge MN, Abiraj K, Schroder CP, Pot L, Bossenmaier B, et al. ImmunoPET and biodistribution with human epidermal growth factor receptor 3 targeting antibody ^{89}Zr-RG7116. MAbs 2014;6:1051–8.
31. Verel I, Visser GW, Boellaard R, Stigter-van Walsum M, Snow GB, van Dongen GA. ^{89}Zr immuno-PET: comprehensive procedures for the production of ^{89}Zr-labeled monoclonal antibodies. J Nucl Med 2003;44:1271–81.
32. Lamberts TE, Menke-van der Houven van Oordt CW, Ter Weele EJ, Bensch F, Smeenk MM, Voortman J, et al. ImmunoPET with anti-mesothelin antibody in patients with pancreatic and ovarian cancer before anti-mesothelin antibody-drug conjugate treatment. Clin Cancer Res 2016;22:1642–52.
33. Eisenhauer EA, Therasse P, Bogaerts J, Schwartz LH, Sargent D, Ford R, et al. New response evaluation criteria in solid tumours: revised RECIST guideline (version 1.1). Eur J Cancer 2009;45:228–47.

34. Loening AM, Gambhir SS. AMIDE: a free software tool for multimodality medical image analysis. Mol Imaging 2003;2:131–7.
35. National Cancer Institute. Common terminology criteria for adverse events. Available at https://wiki.nci.nih.gov/display/VKC/Common+Terminology+Criteria+for+Adverse+Events+FAQ.
36. Lockhart AC, Liu Y, Dehdashti F, Laforest R, Picus J, Frye J, et al. Phase 1 evaluation of ^{64}Cu-DOTA-patritumab to assess dosimetry, apparent receptor occupancy, and safety in subjects with advanced solid tumors. Mol Imaging Biol 2016;18:446–53.
37. Perk LR, Visser GW, Vosjan MJ, Stigter-van Walsum M, Tijink BM, Leemans CR, et al. ^{89}Zr as a PET surrogate radioisotope for scouting biodistribution of the therapeutic radiometals ^{90}Y and ^{177}Lu in tumor-bearing nude mice after coupling to the internalizing antibody cetuximab. J Nucl Med 2005;46:1898–906.
38. Baban DF, Seymour LW. Control of tumour vascular permeability. Adv Drug Deliv Rev 1998;34:109–19.
39. Gebhart G, Lamberts LE, Wimana Z, Garcia C, Emonts P, Ameye L, et al. Molecular imaging as a tool to investigate heterogeneity of advanced HER2-positive breast cancer and to predict patient outcome under trastuzumab emtansine (T-DM1): The ZEPHIR trial. Ann Oncol 2016;27:619–24.
40. Ciprotti M, Tebbutt NC, Lee FT, Lee ST, Gan HK, McKee DC, et al. Phase I imaging and pharmacodynamic trial of CS-1008 in patients with metastatic colorectal cancer. J Clin Oncol 2015;33:2609–16.
41. Liu L. Antibody glycosylation and its impact on the pharmacokinetics and pharmacodynamics of monoclonal antibodies and fc-fusion proteins. J Pharm Sci 2015;104:1866–84.
42. Gaykema SB, de Jong JR, Perik PJ, Brouwers AH, Schroder CP, Oude Munnink TH, et al. ^{111}In-trastuzumab scintigraphy in HER2-positive metastatic breast cancer patients remains feasible during trastuzumab treatment. Mol Imaging 2014;13.
43. Oude Munnink TH, Dijkers EC, Netters SJ, Lub-de Hooge MN, Brouwers AH, Haasjes JG, et al. Trastuzumab pharmacokinetics influenced by extent human epidermal growth factor receptor 2-positive tumor load. J Clin Oncol 2010;28:e355.
44. Bruno R, Washington CB, Lu JF, Lieberman G, Banken L, Klein P. Population pharmacokinetics of trastuzumab in patients with HER2-positive metastatic breast cancer. Cancer Chemother Pharmacol 2005;56:361–9.
45. Weissleder R, Ross B, Rehemtulla A, Gambhir S. Molecular and functional imaging in drug development. In: Molecular imaging principles and practice. 2010th ed. Shelton, Connecticut, USA: People's Medical Publishing House; 2010. p.1161–78.
46. Hulme EC, Trevethick MA. Ligand binding assays at equilibrium: validation and interpretation. Br J Pharmacol 2010;161:1219–37.
47. Kol A, Terwisscha van Scheltinga AG, Timmer-Bosscha H, Lamberts LE, Bensch F, de Vries EG, et al. HER3, serious partner in crime: therapeutic approaches and potential biomarkers for effect of HER3-targeting. Pharmacol Ther 2014;143:1–11.
48. Jaramillo ML, Leon Z, Grothe S, Paul-Roc B, Abulrob A, O'Connor McCourt M. Effect of the anti-receptor ligand-blocking 225 monoclonal antibody on EGF receptor endocytosis and sorting. Exp Cell Res 2006;312:2778–90.
49. Sunada H, Magun BE, Mendelsohn J, MacLeod CL. Monoclonal antibody against epidermal growth factor receptor is internalized without stimulating receptor phosphorylation. Proc Natl Acad Sci USA 1986;83:3825–9.
50. Austin CD, De Maziere AM, Pisacane PI, van Dijk SM, Eigenbrot C, Sliwkowski MX, et al. Endocytosis and sorting of ErbB2 and the site of action of cancer therapeutics trastuzumab and geldanamycin. Mol Biol Cell 2004;15:5268–82.